On the Model Dependence of Kinetic Shifts in Unimolecular Reactions: The Dissociation of the Cations of Benzene and *n*-Butylbenzene[†]

J. Troe,*,‡ V. G. Ushakov,§ and A. A. Viggiano#

Institute for Physical Chemistry, University of Göttingen, Tammannstrasse 6, D-37077 Göttingen, Germany, Institute of Problems of Chemical Physics, Russian Academy of Sciences, 142432 Chernogolovka, Russia, and Air Force Research Laboratory, Space Vehicles Directorate, 29 Randolph Road, Hanscom Air Force Base, Massachusetts 01731-3010

Statistical adiabatic channel model/classical trajectory (SACM/CT) calculations have been performed for transitional mode dynamics in the simple bond fission reactions of $C_6H_6^+ \rightarrow C_6H_5^+ + H$ and $n\text{-}C_6H_5C_4H_9^+ \rightarrow C_7H_7^+ + n\text{-}C_3H_7$. Reduced-dimensionality model potentials have been designed that take advantage of ab initio results as far as available. Average anisotropy amplitudes of the potentials were fitted by comparison of calculated specific rate constants $k(E,J)$ with measured values. The kinetic shifts of the calculated $k(E)$ curves and the corresponding bond energies $E_0(J{=}0)$, derived as 3.90 ± 0.05 eV for $C_6H_6^+$ and 1.78 ± 0.05 eV for $n\text{-}C_6H_5C_4H_9^+$, were in good agreement with literature values from thermochemical studies. Kinetic shifts from fixed tight activated complex Rice–Ramsperger–Kassel–Marcus (RRKM) theory, which also reproduces the measured $k(E)$, were larger than the present SACM/CT results as well as earlier results from variational transition state theory (for $C_6H_6^+$). The approach using RRKM theory was found to underestimate $E_0(J{=}0)$ by about $0.2{-}0.3$ eV. A simplified SACM/CT-based method is also proposed which circumvents the trajectory calculations and allows derivation of $E_0(J{=}0)$ on the basis of measured $k(E)$ and which provides similar accuracy as the full SACM/CT treatment.

1. Introduction

Measurements of specific rate constants $k(E)$ for bond fission processes provide an important access to bond dissociation energies, E_0, of the fragmenting species and, hence, to their thermochemical data. There is no problem when $k(E_0)$ is sufficiently large such that the threshold for fragment appearance can be measured directly. The situation changes when the $k(E)$ at threshold becomes too small to be measured by the available technique and when $k(E)$ has to be extrapolated from energies much above E_0 in order to locate E_0. The determination of E_0 from $k(E)$, that is, the identification of the magnitude of the kinetic shifts of $k(E)$ along the energy axis with respect to E_0, becomes more difficult the larger the dissociating molecule. In this case, suitable models for $k(E)$ have to be designed which allow for the extrapolation to E_0. Often fixed-tight-activated complex Rice–Ramsperger–Kassel–Marcus (RRKM) theory is being used for this type of extrapolation; see, for example, ref 1. It has been shown, however, that approaches considering flexible transition states such as variational transition state theory (VTST) provide considerably different kinetic shifts; see, for example, the VTST modeling of the simple bond cleavage $C_6H_6^+ \rightarrow C_6H_5^+ + H$ in ref 2. The difference in extrapolated E_0 values from RRKM and VTST modeling was as large as 22 kJ mol^{-1} (0.23 eV) for this reaction, indicating that considerable uncertainties in the deduced thermochemical values remained. It, therefore, appears important to carefully inspect the model dependence of kinetic shifts in mass spectrometry. The present article addresses this issue by analyzing in detail two representative simple bond fission reactions, namely

$$C_6H_6^+ \rightarrow C_6H_5^+ + H \tag{1}$$

and

$$n\text{-}C_6H_5C_4H_9^+ \rightarrow C_7H_7^+ + n\text{-}C_3H_7 \tag{2}$$
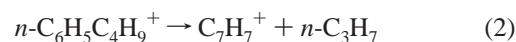
where $C_7H_7^+$ corresponds to benzylium cations.

The transitional mode dynamics are calculated by the statistical adiabatic channel model employing classical trajectory calculations (SACM/CT),[3] specifically the version adapted to ion–molecule reactions.[4] This treatment uses reduced-dimensionality potential energy surfaces for the transitional modes, either from ab initio calculations or from model designs. The transitional mode dynamics is determined by classical trajectories while the dynamics of the conserved modes are treated by SACM calculations that are adiabatic and quantized. The SACM/CT approach was shown to relate dynamical quantities of interest such as $k(E,J)$, thermally averaged rate constants $k_\infty(T)$, and product energy distributions $P(E,J)$ to the potential energy surface in a consistent way (see, e.g., refs 3–5). In the present article, we apply the full SACM/CT approach to reactions 1 and 2. However, we also test simplifications which avoid the tedious trajectory calculations and therefore provide an alternative to RRKM theory that requires the same level of effort.

We have chosen reactions 1 and 2 as examples since previous seminal studies have already provided detailed experimental and theoretical information for these reactions. Specific rate constants $k(E)$ for the dissociation of benzene cations via reaction 1 have

---

been determined over the range of $10^3 – 10^6$ s^{-1} by Dunbar, Klippenstein, Neusser, Schlag, and their co-workers; see refs 2 and 6−9. VTST calculations on a simplified short-range Morse/ long-range electrostatic model potential were performed by Klippenstein, Faulk, and Dunbar in ref 2 while more detailed ab initio calculations of the potential by Klippenstein became available later.[10] Our SACM/CT treatment takes advantage of the ab initio calculations from ref 10 which provide an example for a reaction path potential that has an abrupt change between electronic states. Reaction 1 is also an example for a system with a very small polarizability of the neutral fragment (H) and hence a weak long-range electrostatic potential. Specific rate constants $k(E)$ for the dissociation of *n*-butylbenzene cations have been measured by Baer, Kim, and their co-workers in refs 11 and 12 over the range 2×10^5 to 2×10^9 s^{-1}. Some ab initio calculations of the potential were also performed by Muntean and Armentrout in ref 13 and used to fix a transition state for RRKM calculations of $k(E)$. At the same time, threshold collision-induced dissociation (TCID) measurements were performed in ref 13 and related to $k(E)$ data. Reaction 2 is an example of a system with a much larger polarizability of the neutral fragment (C_3H_7) and hence a stronger long-range electrostatic potential. It appears of interest to compare the kinetic shifts derived by the present technique with those obtained in ref 13, as the TCID studies of Armentrout and co-workers (see refs 13−16 and earlier work cited therein) are intended to improve the accuracy of thermochemical data.

2. Potential Energy Surfaces

Our SACM/CT method approximates that part of the potential, which corresponds to conserved modes, by the potential of separated fragments. This approximation could be improved as indicated in the original version of the SACM,[17] but this would result only in minor changes. Our attention instead focuses on the part of the potential corresponding to transitional modes for which reactant modes turn into external rotations of the separated fragments. The reduced-dimensionality dynamics of the transitional modes is treated explicitly by classical trajectory calculations. In the following, the potential of the transitional modes is represented by a minimum energy path (MEP) potential $V(r)$ as a function of the center-of-mass distance r between the fragments. In addition, the anisotropy, $V(r,\text{angles})$, is of importance since it is responsible for the "rigidity" or "tightness" of the transition state(s). At first, the anisotropy is neglected which provides rate parameters in the limit of phase space theory (PST). Since the complete MEP potential is considered and not exclusively the long-range potential, our PST differs from orbiting transition state theory (OTST).[1,18,19] The potential models of the present work are described individually for the $C_6H_6^+$ and $C_{10}H_{14}^+$ systems below. It should be noted that the zero point of the energy scale is set to the vibrational zero-point level of the separated dissociation products. All calculated quantities are represented at the same energy scale, except the specific rate constants for which the zero point of the energy scale is placed at the vibrational zero-point level of the dissociating reactants.

It should be emphasized that in the present article we focus attention on simple bond fission processes only. We do not treat processes involving tight-activated complexes. These reactions can be characterized by conventional fixed-activated complex RRKM theory such as demonstrated for the channel

$$n\text{-}C_6H_5C_4H_9^+ \rightarrow C_7H_8^+ + C_3H_6 \quad (2a)$$
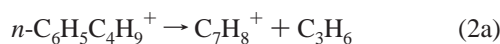
in ref 13.
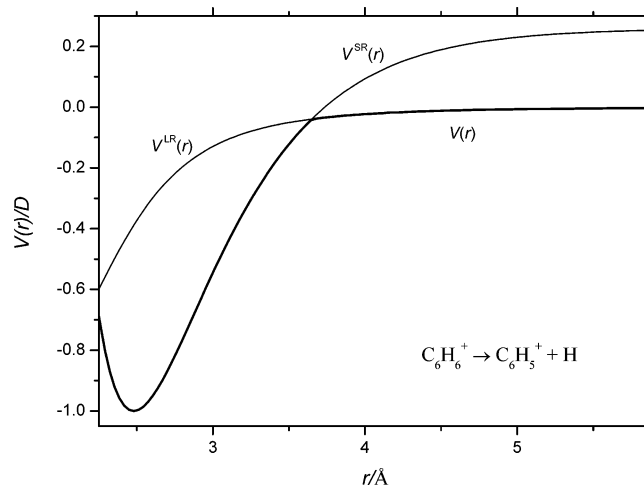
Figure 1. Minimum energy path (MEP) potential $V(r)$ for the dissociation $C_6H_6^+ \rightarrow C_6H_5^+ + H$ (ab initio results for $V(r)$ from ref 10, modeled short-range and long-range potentials $V^{SR}(r)$ and $V^{LR}(r)$ from eqs 3−5 of this work).

2.1. Potential for $C_6H_6^+ \rightarrow C_6H_5^+ + H$. We construct a MEP potential $V(r)$ for this reaction similar to Klippenstein's calculations at the CASPT2 level[10] which shows a Renner− Teller type avoided curve-crossing between a ground $^2B_1$ and an excited $^2A_1$ state of $C_6H_6^+$. Figure 1 shows our modeling of the corresponding $V(r)$. We represent the $^2B_1$ potential inside the curve-crossing by a short-range potential $V^{SR}(r)$ and the $^2A_1$ potential outside the crossing by a long-range potential $V^{LR}(r)$. $V^{SR}(r)$ is approximated by a Morse potential

$$V^{SR}(r) = \Delta E_{ST} + (D + \Delta E_{ST})\{\exp[-2\beta(r - r_e)] - 2\exp[-\beta(r - r_e)]\} \quad (3)$$

where D corresponds to the dissociation energy of $C_6H_6^+$, and ΔE_{ST} is the singlet−triplet splitting of $C_6H_5^+$, that is, the energy difference between the $^2A_1$ and $^2B_1$ states of $C_6H_6^+$ at infinite r. The Morse parameter β from ref 10 follows as $\beta = 1.767$ Å^{-1}, while $r_e = 2.48$ Å represents the sum of a C−C and a C−H distance of 1.4 and 1.08 Å, respectively. ΔE_{ST} is taken as 0.98 eV from ref 10 while $D = 3.90$ eV is our final fitted result; see below. $V^{LR}(r)$ is approximated by a modified ion-induced dipole potential of the form

$$V^{LR}(r) = -(\alpha q^2/2)/[(r - \Delta r_B)^4 + aq^2/2D] \quad (4)$$

with the elementary charge q, the polarizability $\alpha = 0.667$ Å^3 of H atoms, and $\Delta r_B = 1.29$ Å. The latter value has been chosen such that $V^{SR}(r)$ and $V^{LR}(r)$ intersect at the distance $r_{SW} = 3.65$ Å (corresponding to a C−H distance of 2.25 Å such as determined in ref 10) and a crossing at an energy of $-hc$ 1200 cm^{-1}.[10] The MEP radial potential $V(r)$ then follows as

$$2V(r) = V^{SR}(r) + V^{LR}(r) - |V^{SR}(r) - V^{LR}(r)| \quad (5)$$

which gives $-V(r)/hc$ cm^{-1} = 16 600, 1200, 813, 531, 319, 135, and 57 for C−H distances of 1.6, 2.25, 2.5, 2.8, 3.2, 4, and 5 Å, respectively, while the ab initio values from ref 10 were $-V(r)/hc$ cm^{-1} = 18 000, 1200, 830, 600, 350, 130, and 50, respectively.

Some information on the anisotropy of the potential was also obtained in ref 10 by calculating in-plane and out-of-plane force constants as a function of r. As we need a complete reduced-dimensionality potential, we assume an anisotropy model similar to that used in earlier SACM/CT studies (see ref 4 and earlier

Cations of Benzene and *n*-Butylbenzene

J. Phys. Chem. A, Vol. 110, No. 4, 2006 **1493**

references therein) and leave the anisotropy amplitude as a fit parameter. The value needed to fit the experimental $k(E)$ is then compared with the corresponding average value from the ab initio force constants. Our anisotropy model was chosen as

$$2V(r,\theta) = V^{SR}(r) + V^{LR}(r) - \{[V^{SR}(r) - V^{LR}(r)]^2 + \\ 4U^2(\theta)\}^{1/2} + C(1 - \cos\theta)\exp[-\beta(r - r_e)] \quad (6)$$

with

$$U(\theta) = u\sin^2\theta\exp[-\beta(r - r_{SW})] \quad (7)$$

In contrast to $V(r)$, the anisotropy of our model does not show abrupt changes near to the crossing of the two potentials which is in agreement with the force constant calculations from ref 10. We estimated u/hc to be of the order of 1200 cm^{-1}; however, this choice is only of minor significance. On the other hand, the anisotropy amplitude C is of crucial importance since it governs the difference between $k(E)$ and $k(E)$ from PST, denoted by $k^{PST}(E)$. The ratio of C/D and the bond energy D, therefore, are the key parameters of the system which had to be fitted by comparing calculated and measured $k(E)$ values.

2.2. Potential for n-C$_{10}$H$_{14}^+ \rightarrow$ C$_7$H$_7^+$ + C$_3$H$_7$. In contrast to the potential used for C$_6$H$_6^+$dissociation, we assume that the potential of reaction 2 does not involve curve-crossing, is much smoother, and is similar to the potential models used in ref 4. Here we assume that the MEP radial potential can be represented by[4]

$$V(r) = V^{SR}(r)[1 - \kappa F] + V^{LR}(r)F \quad (8)$$

with a switching function

$$F = 1/\{1 + \exp[-2\beta(r - r_{SW})]\} \quad (9)$$

a short-range Morse potential

$$V^{SR}(r) = D\{\exp[-2\beta(r - r_e)] - 2\exp[-\beta(r - r_e)]\} \quad (10)$$

and a modified long-range ion-induced dipole potential

$$V^{LR}(r) = -\frac{\alpha q^2/2}{(r - \Delta r_B)^4 + \alpha q^2/2D} \quad (11)$$

where $\Delta r_B = r_e - r_{Be}$, and r_{Be} is the equilibrium length of the dissociating bond. To obtain a smooth transition between $V^{SR}(r)$ and $V^{LR}(r)$, the parameter κ is modified in comparison to ref 4 by employing

$$\kappa = 1 - \frac{z\alpha q^2}{2D(r_{SW} - \Delta r_B)^4} \quad (12)$$

We have done alternative calculations with stronger or weaker short-range and long-range contributions ($\beta = 5.25$ Å^{-1}, $r_e = 5.27$ Å, $r_{SW} = 5.72$ Å, $r_{Be} = 2.84$ Å, $D/hc = 12\,990$ cm^{-1}, $z = 3$; $\beta = 3.68$ Å^{-1}, $r_{SW} = 5.98$ Å; $\beta = 1.71$ Å^{-1}, $r_{SW} = 6.07$ Å, $r_{Be} = 1.52$ Å changed from the first two potentials, $D/hc = 14\,440$ cm^{-1}, $z = 0.25$; α (C$_3$H$_7$) = 5.8 Å^3, ref 12). Figure 2 shows the first MEP potential while the third MEP potential in Figure 3 reproduces the ab initio points from ref 13. The same rates were calculated with both potential models within error.

It is shown below that the differences between the MEP potentials $V(r)$ are only of small importance while the magnitude of the anisotropy of the potential has a marked influence on the rate. Like in ref 4, we model it by dipole−dipole anisotropy
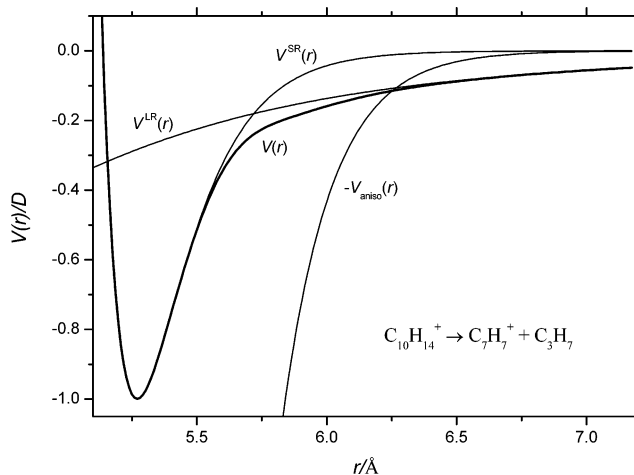
Figure 2. MEP potential $V(r)$ for the dissociation n-C$_{10}$H$_{14}^+ \rightarrow$ C$_7$H$_7^+$ + n-C$_3$H$_7$ (modeling results from eqs 8−12 of this work with parameter set corresponding to $\beta = 5.25$ Å^{-1}; see text. $V_{aniso}(r)$ = anisotropy amplitude from eq 13).
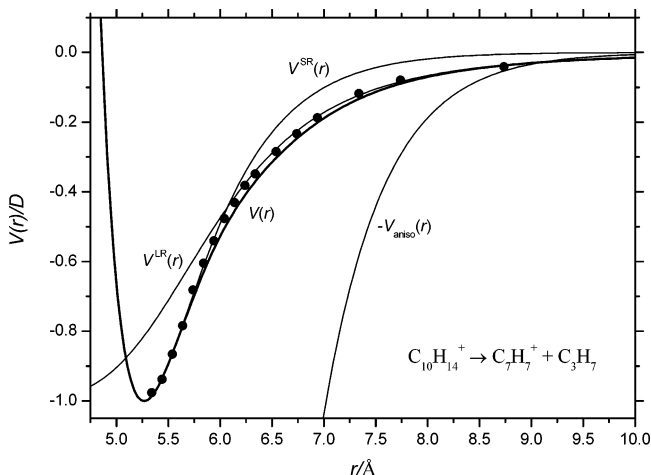

Figure 3. Same as Figure 2, with parameter set corresponding to $\beta = 1.71$ Å^{-1} and ab initio points (●) from ref 13.

$$V(r,angles) = V(r) + C\exp[-\beta(r - r_e)]\{[2 + \mathbf{d}_1\mathbf{d}_2 - \\ 3(\mathbf{d}_1\mathbf{n})(\mathbf{d}_2\mathbf{n})]/4\} \quad (13)$$

where $\mathbf{d}_1$ and $\mathbf{d}_2$ are the unit vectors along the axis of the fragment rotors, $\mathbf{n}$ is the unit vector in the direction of the line connecting the center-of-masses (coms) of the fragments, and C is an effective anisotropy amplitude factor. The r-dependent anisotropy amplitude $V_{aniso}(r) = C\exp[-\beta(r - r_e)]$ is included in Figures 2 and 3 (with C/D = 20) for illustration.

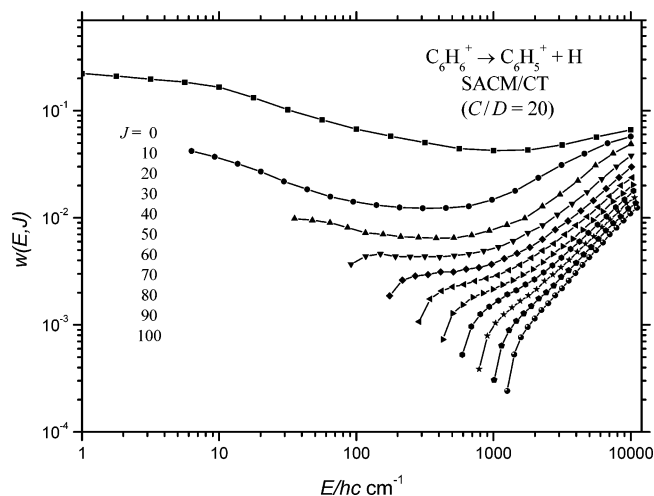## 3. SACM/CT Calculations of Specific Rate Constants $k(E,J)$

The SACM/CT approach explicitly treats the transitional mode dynamics by classical trajectories on the reduced-dimensionality potential energy surfaces described in section 2. This treatment appears particularly necessary because the dynamics is rovibrationally nonadiabatic. This conclusion follows from an inspection of the Massey parameter ξ which corresponds to the ratio between the collision time in the radial potential $V(r)$ and the period of motion of the transitional modes. The Massey parameter for a valence Morse-type potential[4,20] is $\xi = (2\mu B)^{1/2}/\hbar\beta$. For C$_6H_6^+$ one finds $\xi \approx 0.05$ and for C$_{10}$H$_{14}^+$ a range is found, depending on the chosen potential model $\xi \approx 0.1-0.4$. Clearly the condition for adiabatic dynamics, $\xi \gg 1$, is not fulfilled.
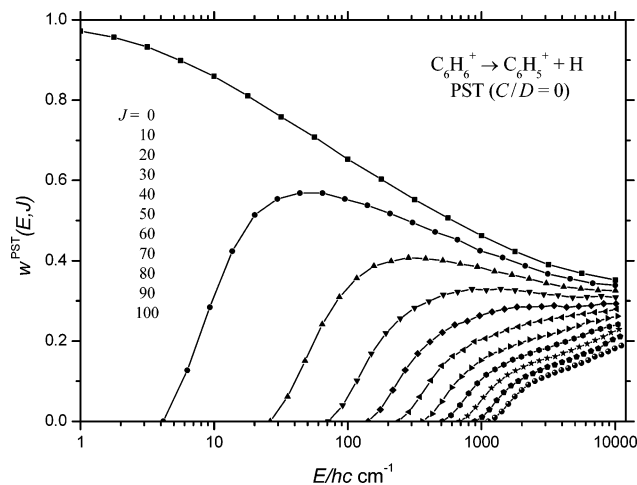
**Figure 4.** Capture probabilities in phase space theory $w^{PST}(E,J)$ for $C_6H_6^+ \rightarrow C_6H_5^+ + H$ (trajectory results for $J = 0$, 10, 20, 30, 40, 50, 60, 70, 80, 90, 100 from top to bottom, anisotropy ratio $C/D = 0$).

Figure 5. Capture probabilities $w(E,J)$ for $C_6H_6^+ \rightarrow C_6H_5^+ + H$ (J values as in Figure 4 but curves with $C/D = 20$).

Figure 6. Specific ridigity factors $f_{rigid}(E,J) = w(E,J)/w^{PST}(E,J)$ for $C_6H_6^+ \rightarrow C_6H_5^+ + H$ (results for $J = 0-50$ with symbols as in Figures 4 and 5; lines are for $C/D = 20$ and points denote $2f_{rigid}(E,J)$ for $C/D = 40$, except $2^{1/2}f(E,J=0)$ for $J = 0$ and $C/D = 40$).

Our calculations follow the approach of trajectories of separated fragments starting from large values of r, where the result is either capture or failure to reach the strongly bound part of the potential. The total number of quantum states of a collision pair with given energy E and total angular momentum (quantum number J) is denoted by $W_0(E,J)$. The capture probability $w(E,J)$ indicates the fraction of $W_0(E,J)$ that reaches the strongly bound range of the potential. $W(E,J) = w(E,J)W_0(E,J)$ then corresponds to the "number of activated complex states" of the transitional modes, if the language of TST or RRKM theory is chosen. $W(E,J)$ finally is convoluted with the contribution of the conserved modes to give the total number $W_{tot}(E,J)$ which enters the well-known expression $k(E,J) = W_{tot}(E,J)/h\rho(E,J)$ from statistical unimolecular rate theory.[1] The Appendix includes all required details for the calculation such as rotational constants and vibrational frequencies of the reactants and dissociation products. We repeat that all quantities are represented in our work with a zero point of the energy scale located at the vibrational zero-point level of the separated dissociation products except $k(E,J)$ for which the zero of the energy scale is placed at the vibrational zero-point level of the dissociating reactant.

3.1. Results for $C_6H_6^+ \rightarrow C_6H_5^+ + H$. If there were no anisotropy of the potential and no centrifugal barriers, $W(E,J)$ would be given by $W_0(E,J)$ such as calculated, for example, in refs 18−23. Introducing the centrifugal barriers $E_0(J)$ of the potential but still neglecting the anisotropy, one obtains capture probabilities in PST denoted by $w^{PST}(E,J)$ such as illustrated in Figure 4 for the $C_6H_6^+$ system. Allowing also for the anisotropy of the potential, one has the final capture probability $w(E,J)$ shown in Figure 5. Details of our CT calculations were described in refs 3 and 4 and are not repeated here. One should note, however, that the number of trajectories was large enough to remove any statistical scatter in the results. The effects of the anisotropy are most easily seen by considering the rigidity factors $f_{rigid}(E,J) = w(E,J)/w^{PST}(E,J)$ shown in Figure 6. At small values of E and J, the comparably weak anisotropy of the long-range potential produces larger values of $f_{rigid}(E,J)$. The final rise at large E values is a consequence of the unusual potential of this system and may be an artifact of our model potential. It appears worth mentioning that the curves of $f_{rigid}(E,J)$ more or less collapse into one curve when they are plotted as a function of $E - E_0(J)$. The corresponding expressions for $f_{rigid}(E,J)$ and $E_0(J)$ are given in the Appendix.
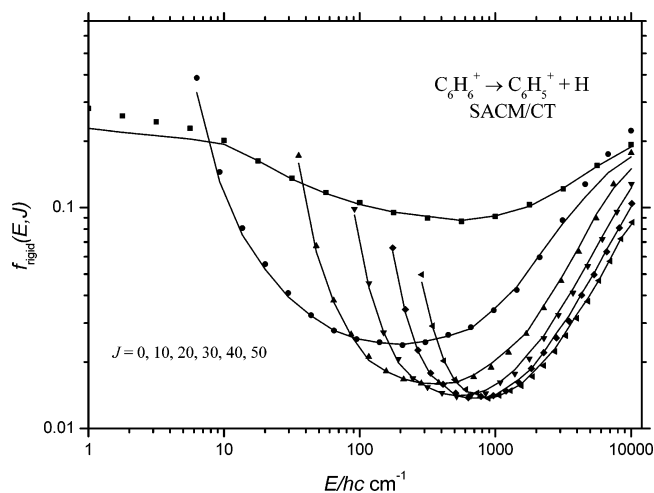
$W(E,J)$, $w(E,J)$, and $f_{rigid}(E,J)$ become smaller as the anisotropy of the potential increases, that is, as the parameter C/D in the potential from section 2 increases. There is a simple scaling of $f_{rigid}(E,J)$ such as demonstrated in Figure 6; the lines correspond to $C/D = 20$ while the points are given by $2f_{rigid}(E,J)$ for $C/D = 40$ (except for the curve with $J = 0$ for which $2^{1/2}f_{rigid}(E,J=0)$ is plotted). Therefore it is easy to fit the final $k(E,J)$ values to the experiments by varying C/D. Figure 7 shows the results. For $C/D = 36$, excellent agreement between the present calculations and the data from refs 2 and 6−9 is obtained when the energy, E, in the experiments is taken as the sum of the photon and total thermal internal energy of $C_6H_6^+$. Figure 7 includes $k(E)$ from PST, that is, calculations with $V(r)$ from section 2.1 with $C/D = 0$. One realizes that $f_{rigid}(E)$ is as small as 10^{-2}, which also corresponds to the minimum of the curves in Figure 6 at $C/D = 40$. The second fit parameter in our approach is the bond energy $E_0(J=0)$, which in Figure 7 was chosen as 3.90 eV. The bond energy corresponds to the horizontal positioning of the $k(E,J)$ curve, and C/D corresponds to the vertical positioning. We discuss the corresponding kinetic shift in section 4. It appears worth mentioning that the ab initio force constants calculated in ref 2 correspond to $C/D = 84$ for

Cations of Benzene and *n*-Butylbenzene

J. Phys. Chem. A, Vol. 110, No. 4, 2006 **1495**
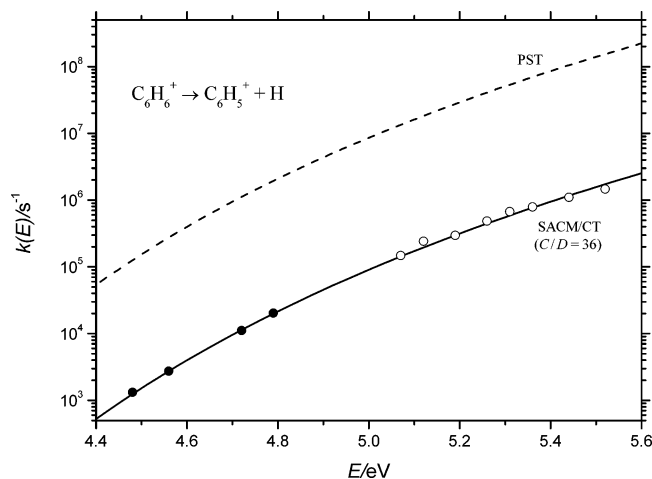
Figure 7. Experimental and modeled specific rate constants $k(E)$ for $C_6H_6^+ \rightarrow C_6H_5^+ + H$ (experimental results from ref 2 (●) and ref 8 (○), $T = 375$ K, full line = SACM/CT modeling with $C/D = 36$ and $E_0(J=0) = 3.90$ eV from this work, dashed line = phase space theory; see text).
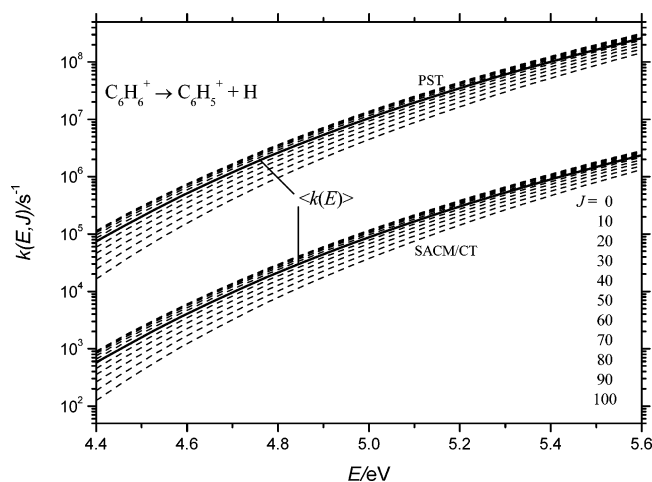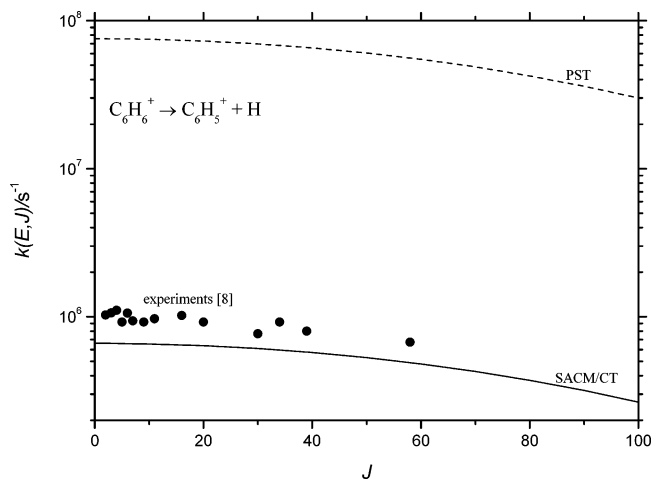

Figure 8. $k(E,J)$ for $C_6H_6^+ \rightarrow C_6H_5^+ + H$ (dashed lines, SACM/CT calculations for $J = 0, 10, 20, 30, 40, 50, 60, 70, 80, 90, 100$ from top to bottom; full line, thermally averaged $k(E)$ for 375 K, see Figure 7; upper curves, phase space theory; lower curves, anisotropic potential with $C/D = 36$, see text).

in-plane and to $C/D = 25$ for out-of-plane bending motions such that the average corresponds well to our fitted value of $C/D = 36$.

For the $C_6H_6^+$ system, an important consistency check can be made by comparing modeled and experimental rotational dependencies of $k(E,J)$. Figure 8 shows our modeled $k(E,J)$ together with the thermally rotationally averaged $\langle k(E,J)\rangle_{375K}$ for the conditions of the experiments from ref 8. One should note that our representations always employ E as the total internal energy. One notices that $k(E,J)$ in this system gradually decreases with increasing J. Figure 9 plots $k(J)$ at a fixed energy of 5.3 eV and demonstrates that our modeled J dependence agrees very well with the experimental results from ref 8. There is a small vertical shift which is due to a small experimental inconsistency between the data from Figures 7 and 9 (the experiments are from ref 8 at 5.3 eV; the SACM/CT curve is optimized to experiments between about 4.5 and 5.5 eV from refs 2 and 8). This could be removed by slightly decreasing C/D, but this would deteriorate the agreement in Figure 7.

The results from our SACM/CT calculations demonstrate that both the experimental E and J dependencies of $k(E,J)$ can very well be modeled for the $C_6H_6^+$ system. In our approach, the

**Figure 9.** $k(E,J)$ for $C_6H_6^+ \rightarrow C_6H_5^+ + H$ (results for total internal energy of 5.3 eV, experimental results (●) from ref 8: full line, SACM/CT calculations from this work; dashed line, phase space theory, see text).
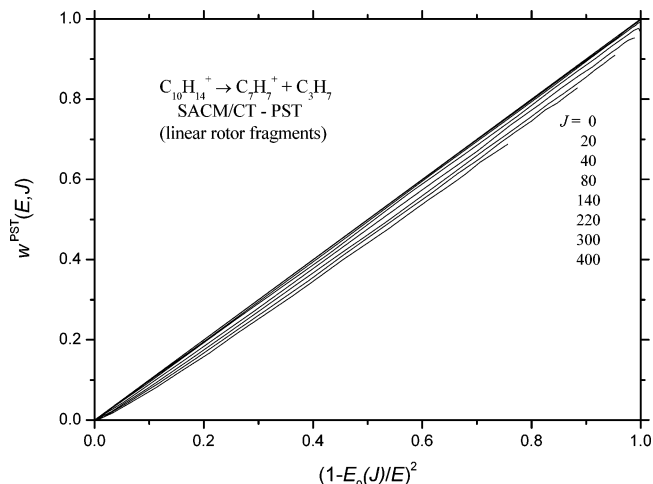

Figure 10. Capture probabilities in phase space theory $w^{PST}(E,J)$ for $C_{10}H_{14}^+ \rightarrow C_7H_7^+ + C_3H_7$ (trajectory calculations treating the products as linear rotors; $E_0(J)$ for model potential with $\beta = 5.25$ Å^{-1}, see Appendix; $J = 0, 20, 40, 80, 140, 220, 300, 400$ from top to bottom).

bond energy $E_0(J=0)$ and the anisotropy parameter C/D have been used as fit parameters. In section 4 we compare the kinetic shifts from our approach with the shifts from other approaches in order to demonstrate the dependence of the shifts on which model is used.

3.2. Results for $C_{10}H_{14}^+$. In this section, we compare our results for $C_{10}H_{14}^+$ with those for $C_6H_6^+$, to demonstrate major system-specific differences. Remember that the potential for $C_6H_6^+$ incorporates a curve-crossing while that for $C_{10}H_{14}^+$ is smoother. In addition, one fragment is an atom in $C_6H_6^+$ while both fragments are polyatomic in $C_{10}H_{14}^+$. The latter property first affects $W_0(E,J)$ (see Appendix) and then $w^{PST}(E,J)$. It was shown in ref 4 that the influence of the centrifugal barriers $E_0(J)$ on $w^{PST}(E,J)$ can be well accounted for by representations of $w^{PST}(E,J)$ as a function of $1 - E_0(J)/E$. However, the appropriate form depends on the character of the fragments. Treating the two fragments in the $C_{10}H_{14}^+$ dissociation (2) as two linear species, one finds that $w^{PST}(E,J)$ is a linear function of $[1 - E_0(J)/E]^2$ such as shown in Figure 10. When two spherical tops are assumed, $w^{PST}(E,J)$ is found to be a linear function of $[1 - E_0(J)/E]^3$; see Figure 11. There is a minor spread in the curves which in part is due to the fact that the approximation $J \approx L$ is not exactly valid (L corresponds to orbital, J to total angular
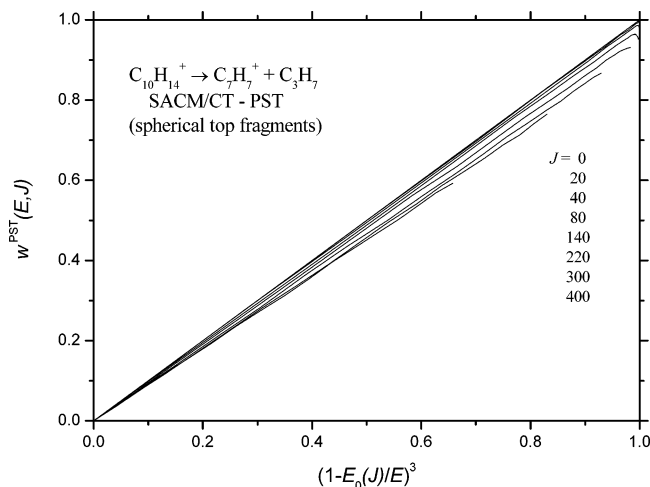
Figure 11. Same as Figure 10 but treating the products as spherical tops (see text).
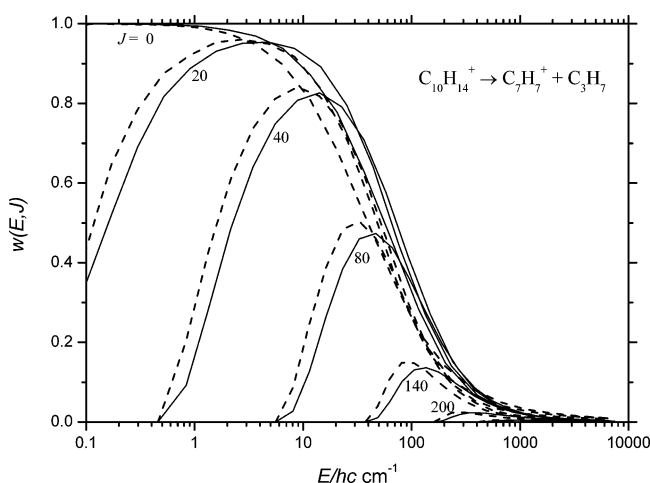

Figure 12. Capture probabilities $w(E,J)$ for $C_{10}H_{14}^+ \rightarrow C_7H_7^+ + C_3H_7$ (SACM/CT results treating the products as spherical tops (solid lines) or linear rotors (dashed lines); $J = 0, 20, 40, 80, 140, 220$ from left to right, $\beta = 5.25$ Å^{-1}, $C/D = 40$, see text).

momentum; our CT calculations statistically sample L for a given J value). Capture probabilities $w(E,J)$ such as shown in Figure 12 for the $C_{10}H_{14}^+$ system markedly differ from those of the $C_6H_6^+$ system illustrated in Figure 5. As a consequence, the rigidity factors $f_{rigid}(E,J)$ shown in Figure 13 also have a different form. Figure 13 shows curves of f_{rigid} as a function of $E - E_0(J)$ for various J values which are almost coincidental. Figure 13 also includes an average rigidity factor $f_{rigid}(E)$ which would reproduce thermal capture rate constants from detailed SACM/CT calculations. These are not presented here. Finally, Figure 14 illustrates that the particular shape of $f_{rigid}(E,J)$ is the same for models employing different Morse parameters β and different molecularities of the fragments (spherical tops in Figure 13 and linear fragments in Figure 14). However, fitting the different models to experimental data for $k(E,J)$ results in different anisotropy parameters, C/D, such as illustrated in the following.

After convolution of the transitional and conserved mode contributions, $W_{total}(E,J)$ and $k(E,J)$ are obtained. Having illustrated the J dependence for the $C_6H_6^+$ system for which measurements are available, we only show $k(E,\langle J \rangle)$ for the $C_{10}H_{14}^+$ system where $\langle J \rangle$ corresponds to an average J value of the experiments. In Figures 15 and 16, experimental $k(E)$ values from refs 11 and 12 are compared with model calculations assuming two linear fragments and two spherical top fragments,
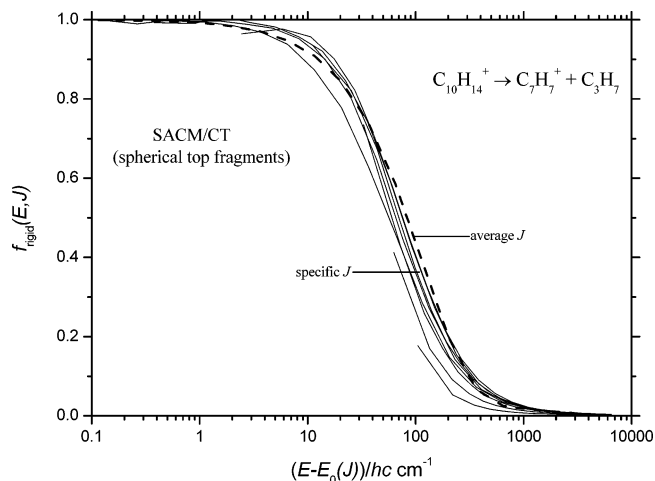
Figure 13. Specific rigidity factors $f_{rigid}(E,J)$ for $C_{10}H_{14}^+ \rightarrow C_7H_7^+ + C_3H_7$ (full lines, SACM/CT calculations with spherical tops for $J = 0$, 20, 40, 80, 140, 200, 300, 400; dashed line, average curve reproducing thermal capture rate and being in the form of eq 14; $\beta = 5.25$ Å^{-1}, $C/D = 40$, see text).
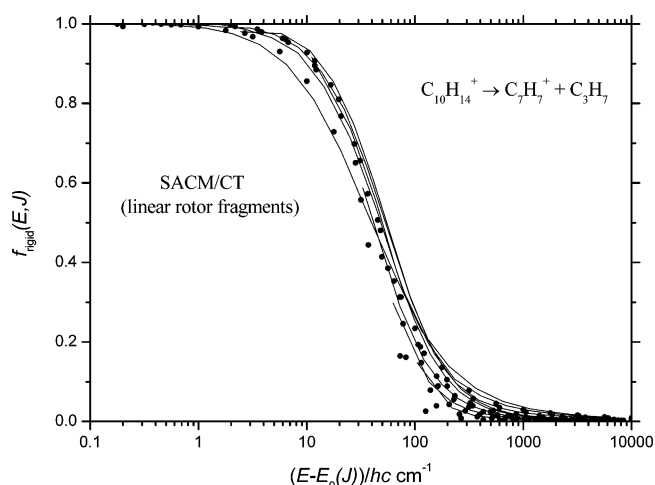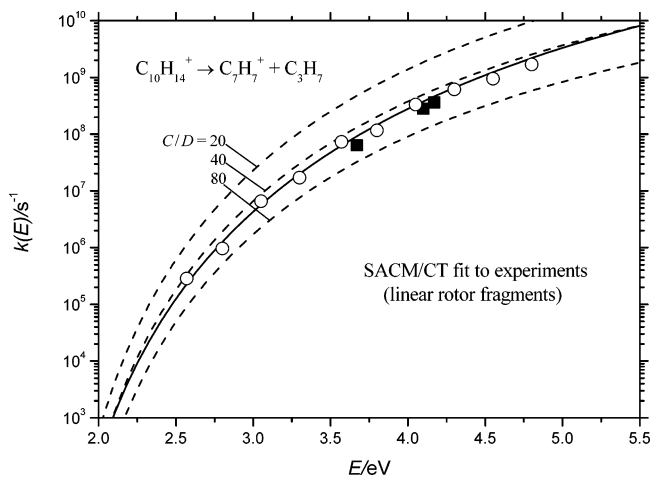

Figure 14. Same as Figure 13 (lines are for linear rotors with $\beta = 5.25$ Å^{-1}, and points are for linear rotors with $\beta = 3.68$ Å^{-1}, $C/D = 40$, see text).

respectively. At a given energy, $k(E)$ decreases with increasing strength of the anisotropy, represented by the ratio C/D. The value of C/D can easily be fitted.

4. Model Dependence of Kinetic Shifts

The SACM/CT calculations from section 3 have shown that E and J dependencies of experimental $k(E,J)$ can be reproduced extremely well by our approach. However, the question arises how well the two fit parameters $E_0(J=0)$ and C/D can be separated, that is, whether the kinetic shift of the curves can be uniquely identified such that $E_0(J=0)$ can be deduced. In addition, it appears of importance to compare the present kinetic shifts with results from calculations from other models. The answer to the first question obviously depends on the range of available experimental data. $E_0(J=0)$ and C/D can be separated in a unique way only when enough curvature in the log $k(E)$ vs E plots has been observed. This seems to be the case for the two systems considered in the present analysis. However, uncertainties in $E_0(J=0)$ on the order of about ± 0.05 eV seem to remain even when careful nonlinear least-squares fits to the experiments are made.

The second question of how the chosen model effects the derived kinetic shifts can also well be answered for the two

Cations of Benzene and *n*-Butylbenzene

J. Phys. Chem. A, Vol. 110, No. 4, 2006 **1497**

Figure 15. Specific rate constants $k(E)$ for $C_{10}H_{14}^+ \rightarrow C_7H_7^+ + C_3H_7$ (dashed lines, SACM/CT calculations for linear rotors with $C/D = 20$, 40, 80 from top to bottom; full line, SACM/CT fit to the experiments from refs 11 (○) and 12 (■) for $\langle J \rangle = 87$.
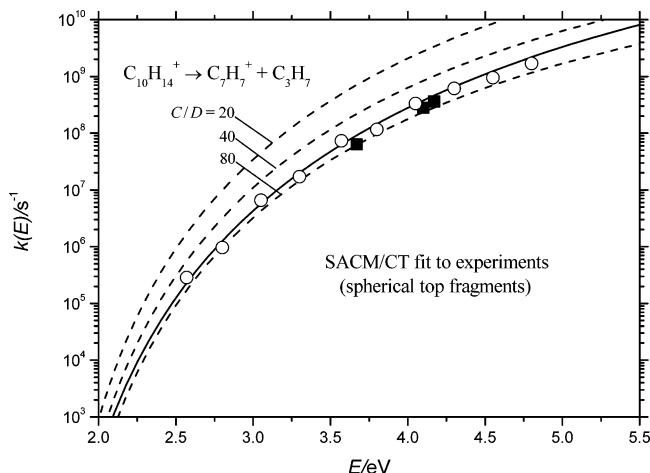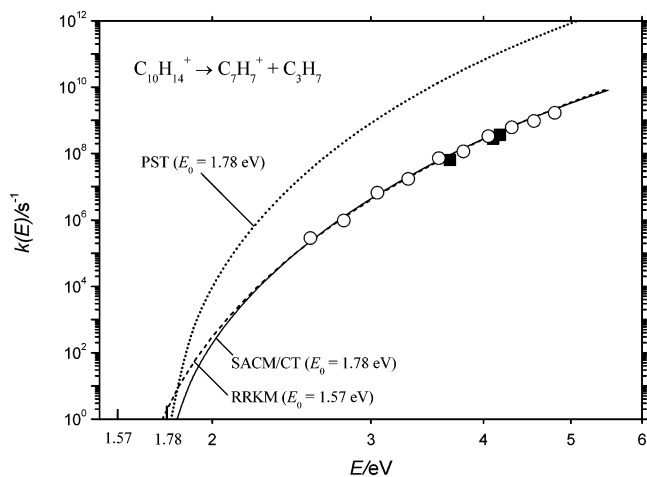

Figure 16. Same as Figure 15 but for spherical tops.
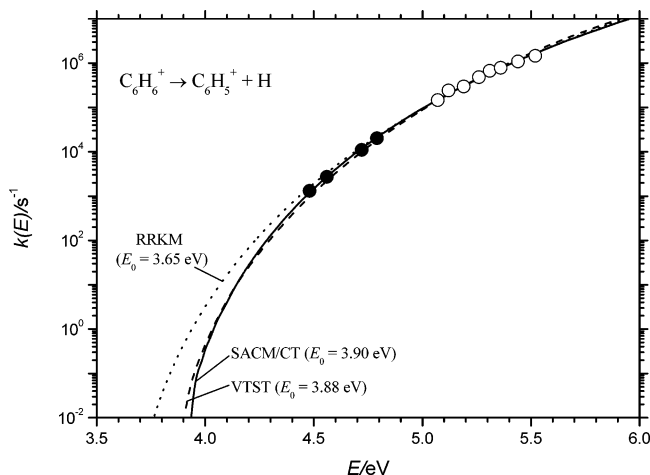
Figure 17. Specific rate constants $k(E)$ for $C_6H_6^+ \rightarrow C_6H_5^+ + H$ from different models fitted to the experimental points of ref 2 (●) and ref 8 (○) (dotted line, fixed-tight-activated complex; dashed line, VTST modeling from ref 2 leading to $E_0(J=0) = 3.88$ eV; full line, SACM/CT modeling from this work leading to $E_0(J=0) = 3.90$ eV, see text.

systems because RRKM and VTST analyses of the measured $k(E)$ values have been made previously and the RRKM analysis has been repeated here to check for consistency. Figure 17 shows (i) the experimental $k(E)$ values for the $C_6H_6^+$ system, which were measured between about 10^3 and 10^6 s^{-1} and which are

Figure 18. Specific rate constants $k(E)$ for $C_{10}H_{14}^+ \rightarrow C_7H_7^+ + C_3H_7$ from different models fitted to the experimental points of ref 11 (○) and ref 12 (■) (dashed line, fixed-tight-activated complex RRKM theory ref 13 leading to $E_0(J=0) = 1.57$ eV; full line, SACM/CT modeling from this work leading to $E_0(J=0) = 1.78$ eV; dotted line, PST with $E_0(J=0) = 1.78$ eV).

markedly above the threshold rate constant $k(E=E_0)$ being $<10^{-2}$ s^{-1}, (ii) an RRKM modeling from ref 6 based on $E_0(J=0)$ = 3.65 eV, (iii) a VTST model which used a simplified short-range/long-range switching model from ref 2 based on $E_0(J=0)$ = 3.88 eV, and (iv) the present SACM/CT model using $E_0(J=0)$ = 3.90 eV. While the curvatures of the plots are nearly the same for the three models in the range of the experimental $k(E)$ values, the fixed-tight-activated complex RRKM model always produces a smaller curvature at smaller energies than that of the SACM/CT and VTST models. As a consequence, the RRKM fit leads to smaller values of the bond energies $E_0(J=0)$. The small difference between the present SACM/CT and the earlier VTST model[2] could be either due to the different potential models or due to some missing dynamical corrections in the VTST calculations. In any case, the VTST and SACM/CT are very close to each other and differ considerably from fixed-tight-activated complex RRKM calculations.

The fitting of modeled to experimental $k(E)$ values leaves an estimated uncertainty of ± 0.05 eV in the extrapolated $E_0(J=0)$ value of 3.90 eV. It appears of interest to compare the derived $E_0(J=0)$ with thermochemical literature values. Combining the dissociation energy 112.0 ± 0.6 kcal mol^{-1} of neutral $C_6H_6 \rightarrow C_6H_5 + H$ at 0 K from ref 24 with the ionization energies of C_6H_6 (9.24378 ± 0.00007 eV) and C_6H_5 (8.32 ± 0.04 eV) from ref 25, leads to $E_0(J=0) = 3.93 \pm 0.05$ eV. This is in excellent agreement with the present value obtained by matching SACM/CT or VTST calculations to the experimental $k(E)$ but not with that obtained from RRKM modeling of $k(E)$.

The differences in modeling kinetic shifts between fixed-tight-activated complex RRKM and SACM/CT approaches is equally pronounced in the $C_{10}H_{14}^+$ system. Figure 18 compares the two fits to the experiments. While both treatments very well reproduce the experimental $k(E)$ values over the range of 10^5-10^9 s^{-1}, they markedly disagree at smaller $k(E)$ values and in the extrapolated $E_0(J=0)$. While the RRKM fit of the experimental $k(E)$ from refs 11 and 12 by Muntean and Armentrout[13] gave $E_0(J=0) = 1.57 \pm 0.10$ eV, being in essential agreement with the RRKM fits from refs 11 and 12 giving 1.61 eV, our SACM/CT fit of the same $k(E)$ led to $E_0(J=0) = 1.78 \pm 0.05$ eV. It should be noted that Muntean and Armentrout also analyzed TCID experiments with competing reactions 2 and 2a or individual dissociation channels in the $C_{10}H_{14}^+$ dissociation.

They derived $E_0(J=0) = 1.70 \pm 0.09$ eV from the former and 1.87 ± 0.10 eV from the latter analysis. However, they used tight optimized fixed transition state structures in combination with RRKM theory. It could well be that an interpretation of TCID data with $k(E)$ for reaction 2 from the present SACM/CT modeling and $k(E)$ from RRKM modeling for reaction 2a such as performed in ref 13 would remove the differences between the derived values. One should also note that the TCID experiments corresponded to energies much closer to threshold than the $k(E)$ measurements. One may finally mention that $E_0(J=0) = 1.80 \, (\pm 0.05)$ eV is the thermochemical value (see the discussion in ref 13) which again is in excellent agreement with the present value of $1.78 \, (\pm 0.05)$ eV.

5. Simplified Approach to Kinetic Shifts

Figures 17 and 18 indicate that a fixed-tight-activated complex RRKM treatment apparently overestimates the kinetic shifts of the $k(E)$ curves while SACM/CT or VTST approaches provide more realistic results. As the trajectory calculations on a model potential of the SACM/CT treatment as well as the VTST approach are both relatively time consuming and in the end require the fit of some potential parameter by comparison with experimental data, one may ask whether the procedure can be simplified. Figures 13 and 14 provide an answer. The dissociations of alkylbenzene cations will all be characterized by potentials which are much more anisotropic at small interfragment distances r than at large values of r. As a consequence, the rigidity factor f_{rigid} will decrease with increasing energy, and an average rigidity factor as a function of $E - E_0(J)$ of the form

$$f_{rigid}(E,J) \approx c_1 + (1 - c_1) \exp\{-[E - E_0(J)]/c_2\} \quad (14)$$

will provide an adequate approximation. Figures 13 and 14 demonstrate this behavior. Figure 13 includes an average rigidity factor which accurately reproduces the thermally averaged capture rate constants determined by detailed SACM/CT calculations. Fitting the parameters c_1 and c_2 by comparison with experimental $k(E)$ values then allows one to circumvent the extensive trajectory calculations. One should, however, keep in mind that other types of anisotropy will require other forms of rigidity factors; see ref 3. However, our experience so far shows that eq 14 will hold also for other ion−molecule reactions.

On the basis of the PST calculations of $k(E,J)$ and $E_0(J)$ calculated from the modeled MEP potential, see Appendix, our fitted results for the parameters c_1 and c_2 were $c_1 = 0$ and $c_2/hc = 203$ cm^{-1} for the $C_6H_6^+$ system and $c_1 = 0.0037$ and $c_2/hc = 125$ cm^{-1} for the $C_{10}H_{14}^+$ system, respectively. The fit is sensitive to the fine details of the measured $k(E)$ and required a nonlinear least-squares analysis of the measured points. In our expression for $f_{rigid}(E,J)$ we neglected the high-energy upturn of $f_{rigid}(E,J)$ for the $C_6H_6^+$ system, see Figure 6, which was not required for fitting $k(E)$ over the experimental energy range and which may also be an artifact of the employed model potential.

The simplified approach to kinetic shifts was found to produce essentially the same results for $k(E,J)$ and the values of $E_0(J=0)$ as the full SACM/CT treatment for these systems. The simplified approach requires the determination of the J dependence of $E_0(J)$ from the MEP potential which has to be done in any case if, for example, thermal capture rate constants are also of interest. It further requires the PST calculation of $k(E,J)$ which involves no more effort than a standard RRKM calculation; see details in Appendix. The merit of the full SACM/CT treatment with

regard to the simplified approach is to determine the functional form of the rigidity factors $f_{rigid}(E,J)$ for the employed type of anisotropy of the potential. We expect that if $k(E)$ is measured over 3 or more orders of magnitude that this approach will be very accurate.

6. Conclusions

The characterization of kinetic shifts of $k(E)$ curves for larger species is an important element in the determination of bond dissociation energies, for example, for molecular ions in mass spectrometry. The present work has shown that the kinetic shifts are model dependent. Fixed-tight-activated complex RRKM theory tends to produce larger kinetic shifts than VTST or SACM/CT treatments in cases of potentials whose anisotropic character changes between short-range valence and long-range electrostatic contributions. We have shown that a fit of SACM/CT based calculations of specific rate constants $k(E)$ to experimental values leads to bond energies $E_0(J=0)$ which are in excellent agreement with literature thermochemical values for the $C_6H_6^+$ and $C_{10}H_{14}^+$ systems. Fixed-tight-activated complex RRKM theory on the other hand underestimates $E_0(J=0)$ by $0.2-0.3$ eV for these systems. The present results are also in excellent agreement with a VTST calculation from ref 2 even though different potentials were used.

The results have important implications for the determination of bond strengths deduced by a variety of ion−molecule techniques (see chapter 5 in ref 26). The present results show that the extrapolation method clearly matters and that more sophisticated theories than RRKM theory should be used for maximum accuracy. With respect to the often used TCID measurements which rely on RRKM calculations to determine the experimental kinetic shift, our analysis shows that the error in the TCID-derived bond energy for the $C_{10}H_{14}^+$ system is not as large as the error in calculating threshold values from $k(E)$ data alone. However, it is expected that incorporating SACM/CT or VTST calculations into the analysis should improve the analysis of those measurements as well.

7. Appendix

Molecular Parameters. 1. Centrifugal barriers $E_0(J)$ (in cm^{-1}, counted above $E_0(J=0)$) $C_6H_6^+$: $E_0(J)/hc$ cm$^{-1} = 1.88 \times 10^{-3} J^4/(1 + 0.114 J^{1.3} + 0.0122 J^2)$. $C_{10}H_{14}^+$: model with $\beta = 5.25$ Å^{-1}, $E_0(J)/hc = 2.47 \times 10^{-7} J^4/(1 + 6.71 \times 10^{-3} J^{1.087} + 5.62 \times 10^{-7} J^{2.387})$; model with $\beta = 3.68$ Å^{-1}, $E_0(J)/hc = 2.47 \times 10^{-7} J^4/(1 + 7.13 \times 10^{-3} J^{1.073} + 8.44 \times 10^{-7} J^{2.347})$; model with $\beta = 1.71$ Å^{-1}, $E_0(J)/hc = 2.47 \times 10^{-7} J^4 (1 + 1.81 \times 10^{-2} J^{0.879} + 3.67 \times 10^{-4} J^{1.601})$.

2. Reactant frequencies (in cm^{-1}) $C_6H_6^+$: 3052, 3049, 3042, 3037, 3033, 3024, 1632, 1500, 1372, 1372, 1347, 1311, 1170, 1149, 1022, 1016, 1015, 1008, 1004, 970, 928, 907, 813, 754, 674, 571, 488, 425, 340, 295 from ref 10. $C_{10}H_{14}^+$: 3177, 3173, 3162, 3156, 3155, 3082, 3072, 3061, 3058, 3031, 3022, 3010,

Cations of Benzene and *n*-Butylbenzene

J. Phys. Chem. A, Vol. 110, No. 4, 2006 **1499**

2995, 2993, 1639, 1517, 1505, 1497, 1487, 1484, 1476, 1459, 1397, 1395, 1382, 1336, 1328, 1285, 1280, 1252, 1236, 1226, 1202, 1196, 1160, 1092, 1053, 1051, 1004, 995, 986, 986, 982, 976, 948, 879, 847, 805, 789, 777, 767, 732, 627, 541, 527, 435, 364, 361, 343, 244, 234, 179, 119, 69, 64, 40 from ref 13.

3. Product frequencies (in cm^{-1}) $C_6H_5^+$: 3128, 3112, 3075, 3125, 3078, 1747, 1461, 1429, 1288, 1257, 1177, 1107, 1063, 1043, 974, 939, 849, 862, 861, 769, 650, 628, 453, 401, 349, 346, 260 from ref 10. $C_7H_7^+$: 3209, 3178, 3176, 3158, 3156, 3152, 3115, 1644, 1578, 1555, 1485, 1458, 1404, 1370, 1336, 1197, 1187, 1120, 1085, 1032, 1007, 995, 984, 984, 972, 835, 808, 785, 632, 617, 599, 524, 411, 352, 336, 162 from ref 13. C_3H_7: 3193, 3098, 3059, 3051, 3001, 2984, 2966, 1506, 1495, 1485, 1462, 1398, 1320, 1300, 1186, 1083, 1014, 893, 884, 738, 512, 328, 247, 77 from ref 13 (introducing one omitted frequency 893).

4. Rotational constants (in cm^{-1}) $C_6H_6^+$: $A_e = 0.0931$, $B_e = (0.193 \times 0.179)^{1/2}$, $\sigma = 6$, $g_{el}(C_6H_6^+) \approx 4$, $g_{el}(H) = 2$. $C_6H_5^+$: $B_e = (0.180 \times 0.226 \times 0.100)^{1/3}$, from ref 10. $C_6H_6^+$ was treated as a spherical or symmetric top in calculations of densities of states $\rho(E,J)$ using the Whitten–Rabinovitch algorithm.[1] $C_6H_5^+$ was mostly treated as spherical top in SACM/CT calculations, employing state counting for conserved modes and convolution with the SACM/CT contributions for transitional modes. An anharmonicity factor of 1.4 was used in $\rho(E,J)$ like in ref 2. $C_{10}H_{14}^+$: $A_e = 0.116$, $B_e = 0.019$. $C_7H_7^+$: $A_e = 0.178$, $B_e = 0.75$, $\sigma = 2$. C_3H_7: $A_e = 1.044$, $B_e = 0.278$ from ref 13. For calculations of densities of states $\rho(E,J)$ and numbers of open channels $W(E,J)$, the analogous procedures were employed as for $C_6H_6^+$.

References and Notes

(1) Baer, T.; Hase, W. L. *Unimolecular Reaction Dynamics. Theory and Experiments*; Oxford University Press: Oxford, U.K., 1996.

(2) Klippenstein, S. J.; Faulk, J. D.; Dunbar, R. C. *J. Chem. Phys.* **1993**, *98*, 243.

(3) Maergoiz, A. I.; Nikitin, E. E.; Troe, J.; Ushakov, V. G. *J. Chem. Phys.* **2002**, *117*, 4201.

(4) Troe, J.; Ushakov, V. G.; Viggiano, A. A. *Z. Phys. Chem.* **2005**, *219*, 715.

(5) Troe, J.; Ushakov, V. G.; Viggiano, A. A. *Z. Phys. Chem.* **2005**, *219*, 699.

(6) Kühlewind, H.; Kiermeier, A.; Neusser, H. J. *J. Chem. Phys.* **1986**, *85*, 4427.

(7) Kühlewind, H.; Kiermeier, A.; Neusser, H. J.; Schlag, E. W. *J. Chem. Phys.* **1987**, *87*, 6488.

(8) Kiermeier, A.; Kühlewind, H.; Neusser, H. J.; Schlag, E. W.; Lin, S. *J. Chem. Phys.* **1988**, *88*, 6182.

(9) Neusser, H. J. *J. Phys. Chem.* **1989**, *93*, 3897.

(10) Klippenstein, S. J. *Int. J. Mass Spectrom. Ion Processes* **1997**, *167/168*, 235.

(11) Baer, T.; Dutuit, O.; Mestdagh, H.; Rolando, C. *J. Phys. Chem.* **1988**, *92*, 5674.

(12) Oh, S. T.; Choe, J. C.; Kim, M. S. *J. Phys. Chem.* **1996**, *100*, 13367.

(13) Muntean, F.; Armentrout, P. B. *J. Phys. Chem. A* **2003**, *107*, 7413.

(14) Rodgers, M. T.; Ervin, K. M.; Armentrout, P. B. *J. Chem. Phys.* **1997**, *106*, 4499.

(15) Rodgers, M. T.; Armentrout, P. B. *J. Chem. Phys.* **1998**, *109*, 1787.

(16) Muntean, F.; Armentrout, P. B. *J. Phys. Chem. B* **2002**, *106*, 8117.

(17) Quack, M.; Troe, J. *Ber. Bunsen-Ges. Phys. Chem.* **1974**, *78*, 240.

(18) Chesnavich, W. J.; Bowers, M. T. *J. Chem. Phys.* **1977**, *66*, 2306.

(19) Chesnavich, W. J.; Bowers, M. T. In *Gas-Phase Ion Chemistry*; Bowers, M. T., Ed.; Academic Press: New York, 1979; Vol. 1, p 119.

(20) Nikitin, E. E.; Troe, J. *Ber. Bunsen-Ges. Phys. Chem.* **1997**, *101*, 445.

(21) Troe, J. *J. Chem. Phys.* **1983**, *79*, 6017.

(22) Olzmann, M.; Troe, J. *Ber. Bunsen-Ges. Phys. Chem.* **1992**, *96*, 1327.

(23) Olzmann, M.; Troe, J. *Ber. Bunsen-Ges. Phys. Chem.* **1994**, *98*, 1563.

(24) Davico, G. E.; Bierbaum, V. M.; DePuy, C. H.; Ellison, G. B.; Squires, R. R. *J. Am. Chem. Soc.* **1995**, *117*, 2590.

(25) *NIST Chemistry Webbook;* Linstrom P. J., Mallard, W. G., Eds.; NIST Standard Reference Data Base No 69; NIST: Gaithersburg, MD, 2005. http://webbook.nist.gov.

(26) *The Encyclopedia of Mass Spectrometry Vol. 1.*; Gross, M., Caprioli, R., Armentrout, P., Eds.; Elsevier: Amsterdam, The Netherlands, 2003.